OPEN

PRS GLOBAL OPEN EXPERIMENTAL

Nrf2-activating Therapy Accelerates Wound Healing in a Model of Cutaneous Chronic Venous Insufficiency

Joseph Kuhn, MD
Darren L. Sultan, MD
Bukhtawar Waqas, BA
Trevor Ellison, MD
Jennifer Kwong, BA
Camille Kim, DPM
Absara Hassan
Piul S. Rabbani, PhD
Daniel J. Ceradini, MD

Background: Chronic venous insufficiency (CVI) stems from venous hypertension, extravasation of blood, and iron-rich skin deposits. The latter is central to ulcer development through generating reactive oxygen species (ROS) that drive persistent local inflammation and the development of lipodermatosclerosis. The ability to study CVI cutaneous inflammation is fundamental to advancing therapies. To address this end, a novel protocol was adapted to investigate cutaneous wound healing in iron-induced inflammation.

Methods: Mice were injected subcutaneously or intraperitoneally with iron-dextran, and excisional wounding was performed. Histologic and biomolecular analysis was performed.

Results: Iron loading was associated with dense iron deposits similar to those in chronic venous stasis. Subcutaneous but not intraperitoneal loading resulted in dermal collagen expansion. Iron overload was associated with atypical antioxidant expression as compared to vehicle controls ($p < 0.0001$) as well as delayed wound healing by 3-4 days. A potent activator of Nuclear factor erythroid 2-related factor 2 (Nrf2), a major transcriptional regulator of redox status, was applied to establish therapeutic efficacy. Nrf2 activation in the wound resulted in significant reduction of closure times across all experimental arms. Antioxidant expression following topical treatment was significantly increased for intraperitoneally iron-loaded mice ($p < 0.0001$) but did not achieve significance for the subcutaneously-loaded animals.

Conclusions: We have characterized a novel model of cutaneous iron-overload designed to advance our understanding of dysfunctional wound healing in CVI. Cutaneous changes of iron overload coincide with redox imbalance and delayed wound healing. By activating Nrf2, we demonstrate the regenerative potential of pro-antioxidant mediators in treating CVI related wound complications. *(Plast Reconstr Surg Glob Open 2020;8:e3006; doi: 10.1097/GOX.0000000000003006; Published online 25 November 2020.)*

INTRODUCTION

Chronic venous insufficiency (CVI) is an increasingly significant public health care problem that contributes to more than 2% of national health expenditures in Western countries.[1] Estimates of CVI prevalence among adults vary widely by regions, with figures ranging from 57.1% to 90.4%.[2–5] The progression of CVI to ulcers accounts for a major share of the economic burden of the disease. Major risk factors for the development of CVI include obesity and age, raising concerns about an increasing incidence over time of both CVI and clinically advanced CVI.[6–8] Limited attempts have been made to identify novel pathologic targets, and innovative biologic therapies offer the promise of addressing CVI's unique pathophysiologic features.[9]

The pathophysiology of CVI originates with aberrantly increased pressures within the venous system as a result of

From the Hansjörg Wyss Department of Plastic Surgery, NYU Langone Health, New York, N.Y.

Received for publication May 22, 2020; accepted June 3, 2020.

DOI: 10.1097/GOX.0000000000003006

Disclosure: *Dr Ceradini has received compensation as a clinical consultant for Reata Pharmaceuticals but holds no stock, shares, equity, or intellectual property rights for the compounds used in this study. Reata Pharmaceuticals provided the RTA 408 but was not part of design, execution, analysis, or interpretation of this study. All the other authors have no financial interest to declare.*

Related Digital Media are available in the full-text version of the article on www.PRSGlobalOpen.com.

obstruction or reflux.[10] The latter forces contribute to elevated venous hydrostatic forces and relative hypoxia due to poor venous return. The unifying pathologic mechanism of the various forms of advanced CVI is one of endothelial dysfunction driving local inflammation.[11–13] Accordingly, drug therapies designed to treat clinically significant CVI often target endothelial activation and the resulting inflammatory cascade.[14–16] The clinical signs of CVI are most apparent in the overlying skin, which is the site of critical morbidity in the form of poorly healing chronic ulcers. Understanding the role of inflammation in the development of such chronic wounds is paramount to their treatment.

In addition to the inflammation stemming from increased shear stress and an activated endothelium, the extravasation of immune cells into the surrounding dermis perpetuates tissue damage within the skin.[17,18] Iron overload in mice has been shown to induce proinflammatory macrophage M1 polarization and fibrogenesis within the liver.[19] In skin, there appears to be a similar correlation between iron overload and ulcer development, and this association is exacerbated by relevant genetic or environmental factors.[20–23] Subsequent studies highlight the role of reactive oxygen species (ROS) from iron deposits as a major driver of the local inflammatory milieu.[24] This understanding helps clarify a number of potential therapeutic targets that can be exploited for amelioration of chronic wounds in CVI.

The ability to test such pharmacotherapies efficaciously relies on the creation of reproducible animal models. Intraperitoneal iron–dextran loading of mice has been shown to be a useful model for studying hepatic iron overload.[25] Sindrilaru et al[26] expanded this approach to the study of impaired cutaneous wound healing in the setting of ROS burden from the iron overload. However, there are limitations for this approach in the confounding of systemic effects of intraperitoneal iron loading. We therefore propose an adapted model for investigating the effect of iron overloading in cutaneous wound healing based on subcutaneous iron–dextran injection. The model also includes the use of stents to humanize the murine wounds, which are otherwise governed by significant contractile forces.[27] Previous work by our group demonstrates that potent Nrf2 activators help alleviate dysfunctional wound healing that stems from the elevated ROS burden associated with diabetes.[28] Using a novel model of cutaneous iron overload, we highlight the benefits of modulating redox homeostasis via Nrf2 for cutaneous wound healing in a murine model of CVI.

MATERIALS AND METHODS

Human Tissue Samples

All samples were procured from discarded tissues of surgical specimens of patients with chronic venous stasis wounds. All samples were completely anonymized and provided by the Dermatological Pathology Department at NYU, in accordance with the Declaration of Helsinki.

Mice

C57BL/6 strains were purchased from Jackson Laboratories (Bar Harbor, Maine) and used for wounding. Mice were housed and fed per the standard protocols. All experiments were approved by the Institutional Animal Care and Use Committee at New York University School of Medicine.

Iron Loading

Six- to eight-week-old mice were injected either intraperitoneally (IP) or subcutaneously (SC) in the dorsal skin with 5 mg iron–dextran at 200 μL per 20 g mouse or 200 μL PBS–dextran (Sigma-Aldrich). SC injections were performed along the dorsolateral aspect of the mid back at 2 locations. This was repeated every 3 days for 21 days, as previously described for IP injections.[26] Before each injection, the mice were anesthetized with inhalational isoflurane and photographed.

Skin Tissue Histology

Animals from each experimental group were sacrificed following day 21 of the injection protocol. Dorsal skin was excised, and fixation was performed overnight using 4% paraformaldehyde, followed by 3 washes in 1× PBS. Fixed samples were then embedded into paraffin using standard histologic processing. After deparaffinization, 5-μm sections were stained with hematoxylin and eosin (H&E), Perls' Prussian blue dye, or trichrome dyes, depending on the experiment. The sections were then photographed, and the image brightness and contrast were adjusted with ImageJ (NIH, Bethesda, Md.). Epithelial gap was calculated as the horizontal distance in pixels between 2 wound epithelial edges on H&E-stained tissue sections, using ImageJ. Dermal collagen depth, in pixels, is the vertical depth of the collagen staining as a percentage of the total depth of the tissue from epidermis to panniculus carnosus, based on trichrome staining and using ImageJ.

8-Hydroxy-2′-deoxyguanosine Measurement

8-Hydroxy-2′-deoxyguanosine (8-OhdG) was measured with Oxidative DNA Damage ELISA Kit (Cell Biolabs, San Diego, Calif.) as per the manufacturer's instructions. Briefly, 96-well plates were coated with 8-OHdG-BSA/PBS conjugate overnight at 4°C. After washes, the plates were blocked with assay diluent for 1 hour at room temperature. Samples and standards were incubated for 10 minutes, followed by incubation with anti-8-OHdG antibody for 1 hour. After washing, horseradish peroxidase–coupled secondary antibody was incubated for 1 hour. After several washes, peroxidase-substrate solution was added. The reaction was stopped after 5 minutes, measurements were taken at 450 nm on the Synergy-H1 plate reader (Biotek, Winooski, Vt.), and the readings were standardized to total DNA.

Quantitative RT-PCR

Total RNA was isolated from dorsal back skin following the 21-day injection protocol and additionally from the 10-day-old wound tissue after treatment with topical agents. The RNeasy kit (QIAGEN, Calif.) was used for this extraction, with a few modifications. Skin or wound bed samples were mechanically chopped in 1 mL Trizol (Life Technologies, Calif.) and homogenized using a Polytron

tissue homogenizer (Kinematica, N.Y.). Two hundred microliters of chloroform was added and agitated, to allow for phase separation, and the aqueous phase was drawn off after centrifugation at 12,000*g* for 15 minutes at 4°C. RNA was precipitated by the addition of equal volume of isopropanol and incubation on ice for 30 minutes. Suspensions were loaded onto spin columns of the RNeasy kit and the remaining steps were carried out as per the kit protocol. Reverse transcription was carried out with 500 ng of eluted RNA using the high-capacity cDNA synthesis kit (4368814; Applied Biosystems, Calif.). Primers specific for *manganese superoxide dismutase (MnSOD), NAD(P)H quinone dehydrogenase 1 (NQO1),* and *heme oxygenase 1 (HO-1)* transcripts were used in addition to *18s* controls. Real-time quantitative PCR was performed using SYBR Green Master Mix (4364344, Life Technologies, N.Y.) and the QuantStudio 7 Flex (Applied Biosystems) thermocycler. Relative expression of mRNA levels was calculated by the delta-delta CT method.

Cutaneous Wounding Model

A previously described excisional wound healing model was used for murine cutaneous wounds.[27] Briefly, mice were anesthetized using inhalational isoflurane, and the dorsal hairs were removed using clippers and Nair. A 10-mm-diameter punch biopsy was used to create full-thickness wounds extending through the panniculus carnosus. 0.5-mm-thick silicone circular stents (665581; Sigma-Aldrich, Mo.) were sutured to the wound edges with interrupted 4–0 silk sutures (Ethicon, Inc., N.J.) to prevent wound contraction. Standardized photographs were taken on postwounding days 0, 7, 10, 14, 17, and 18. The percent of the remaining wound area was calculated relative to the internal diameter of the stents to correct for magnification or other photographic effects. These calculations were performed digitally (ImageJ, NIH), with the observer blinded to the treatment method. Subsequent area under the curve (AUC) analysis was performed by the trapezoidal rule (GraphPad Prism). AUC determined wound burden. Pathologic wound burden was defined as an increase in AUC over the physiologic wound burden or the AUC of the vehicle or untreated arm.

Preparation of Topical Nrf2 Activator

Nrf2 activator, RTA 408 (omaveloxolone) (Reata Pharmaceuticals, Irving, Tex.) was stored at 4°C. Solutions were prepared for daily use preceding each application. 1.0% RTA 408 suspension was prepared in sesame oil and diluted to prepare the 0.1% RTA 408 preparation. Aggressive vortexing ensured adequate solution uniformity before dilution and application. In a blinded fashion, 50 μL of sesame oil, 0.1% RTA 408, or 1.0% RTA 408 was added dropwise to the dorsal wounds following solution preparation.

Statistical Analysis

All data are based on a minimum of triplicate analysis, unless otherwise noted. Data are represented as mean ± error or SD. Analyses were performed using analysis of variance and multiple pairwise comparisons. $P < 0.05$ is considered significant, and lower P values are indicated.

RESULTS

Iron Loading in Mice Simulates the Cutaneous Iron Burden Found in Human Venous Stasis

After 21 days of iron loading by either IP or SC routes, red-orange discoloration appears over the dorsal skin (Fig. 1A). (**See figure, Supplemental Digital Content 1**, which displays iron–dextran loading of mouse skin leads to hemosiderin deposits. A, Schematic of iron loading course and dosing. B, Photographs of dorsal skin of mice over 21 days of either IP or SC injections of iron–dextran. C, Higher magnification H&E-stained histology of mouse skin with IP or SC iron loading for 21 days compared with dextran-loaded control mouse skin and human tissue from a case with chronic venous stasis. N = 5 for all mouse groups, **http://links.lww.com/PRSGO/B437**.) In the IP cohort, iron deposits, which present as a rusty hue in gross phenotype, are most noticeable after the ninth day, in comparison to the sixth day in the SC loading cohort. Tissue elasticity was relatively preserved in the intraperitoneal injection cohort as demonstrated by the ease of skin tenting during clinical examination of treated animals at day 21 (not shown). SC injection, by contrast, resulted in thick, shiny skin with discernable superficial veins more akin to the cutaneous stigmata of chronic venous stasis noted in humans. Correspondingly, hemosiderin deposits became apparent in the dermal and adipose compartments of

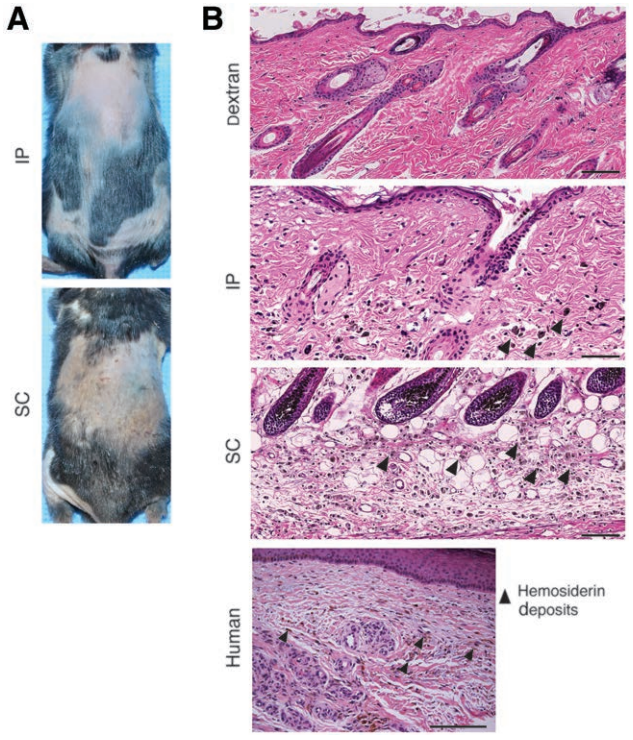

Fig. 1. Iron–dextran loading of mouse skin leads to hemosiderin deposits. A, Photographs of dorsal skin of mice at 21 days after either IP or SC injections of iron–dextran. B, H&E-stained histology of mouse skin with IP or SC iron loading for 21 days compared with dextran-loaded control mouse skin and human tissues from a case with chronic venous stasis. Black arrowheads indicate hemosiderin deposits. n = 5 for all mouse groups.

skin tissue sections of iron–dextran–loaded mice but were absent in those of only dextran-loaded mice (Fig. 1B). These intracellular deposits closely resemble those found in human venous stasis, where extruded red blood cells are digested by tissue macrophages, leaving behind iron-rich deposits that appear brown on H&E staining. Interestingly, iron loading through the IP cavity of mice resulted in slightly less-concentrated hemosiderin deposits than after SC iron loading.

Subcutaneous Iron Loading Is Associated with Poor Skin Quality and Dermal Collagen Expansion

Photographic analysis of mouse skin tissue sections demonstrates marked histologic differences dependent on the method of iron loading by either IP or SC injections (Fig. 2) (**see figure, Supplemental Digital Content 2**, which displays iron–dextran loading of mouse skin alters skin histology. A, Higher resolution Perls' Prussian blue staining of IP and SC iron-loaded skin after 21 days and human skin tissue with chronic venous stasis. Iron deposits appear in blue. B, Higher resolution trichrome staining of skin sections following IP and SC iron loading or dextran control. Collagen stains a deep blue color. n = 5 for all treatment groups, **http://links.lww.com/PRSGO/B438**). Perls' Prussian blue staining, which allows for direct visualization of iron deposits, demonstrated that iron deposition is strikingly higher in SC-loaded mouse skin compared with IP-loaded mouse skin. The iron deposits in both the loading routes bear resemblance to pathologic human skin with chronic insufficiency (Fig. 2A). Trichrome staining showed that SC injection resulted in increased dermal collagen, as well as a thicker dermis, evidenced by the higher intensity of blue dye, compared with IP injection (Fig. 2B) (**see figure, Supplemental Digital Content 3**, which displays characterization of iron-loaded skin and establishment of a model for delayed wound healing secondary to chronic venous stasis. A, Quantification of increased collagen in intact skin following iron loading, represented by the depth of collagen on trichrome staining, n = 5. B, Relative fold change of 8-OHdG in IP–iron, SC–iron, and dextran-loaded mouse skin, n = 3. C, Representative images of stented excisional wounds on IP–iron–dextran, SC–iron–dextran, and dextran-loaded mouse skin. d = days, **http://links.lww.com/PRSGO/B439**). The increased collagen in the superficial layers of the skin may underlie some of the macroscopic findings above. Our results thus far demonstrate that iron loading in mice, whether by IP or SC route, can recapitulate the phenotypes of skins associated with CVI.

Iron Loading Is Associated with Altered Antioxidant Gene Expression and Delayed Cutaneous Wound Healing

To investigate the molecular changes induced by IP or SC iron loading, we assessed the levels of oxidative DNA damage indicated by 8-OHdG. IP and SC iron loading led to increases in 8-OHdG by 11% and 15%, respectively, when compared with dextran loading. However, the 8-OHdG levels did not reach significance (SDC3B). MnSOD and NQO1 are both redox-sensitive enzymes that contribute to restoration and maintenance of homeostasis in the setting of oxidative stress. Expression of MnSOD was significantly higher in iron-loaded skin when compared with dextran-loaded controls ($P < 0.0001$), and this increase was consistent with both the routes of iron loading (Fig. 3A). NQO1, in contrast, was significantly downregulated ($P < 0.0001$) in mouse skin after iron

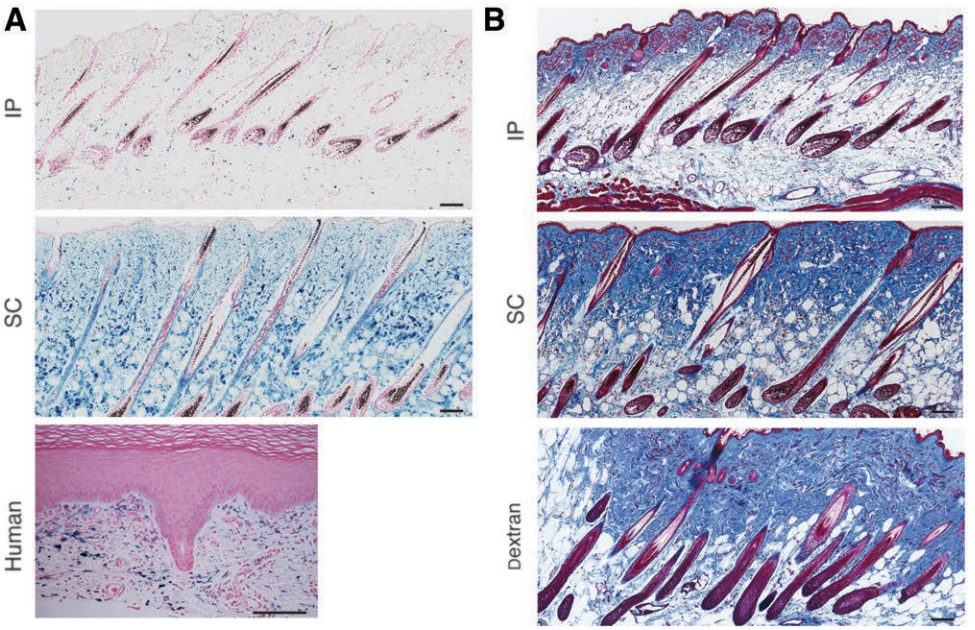

Fig. 2. Iron–dextran loading of mouse skin alters skin histology. A, Perls' Prussian blue staining of IP and SC iron-loaded skin after 21 days and human skin tissues with chronic venous stasis. Iron deposits appear in blue. B, Trichrome staining of skin sections following IP and SC iron loading or dextran control. Collagen stains a deep blue color. n = 5 for all treatment groups.

loading (Fig. 3A). To investigate whether the iron loading led to delays in cutaneous wound healing, as observed in human patients, full-thickness wounds were generated on the dorsum of iron-loaded mice and monitored to closure (SDC3C). IP or SC iron loading significantly delayed wound healing by 3–4 days, requiring 18 days to close compared with the 14 days of dextran-loaded control wounds (Fig. 3B). By determining the percent of the wound area remaining over time, it is possible to graphically represent the wound burden by integrating the AUC (Fig. 3C). SC iron loading led to the greatest increase in wound burden by 23%, over the dextran-loaded control wound burden, while IP iron loading resulted in a 15% increase in pathological wound burden (Fig. 3C,D). Our data suggest that iron loading leads to dysregulation of antioxidant cytoprotective mechanisms and contributes to pathologic wound healing.

Topical Nrf2 Activation Prevents the Delay in Cutaneous Wound Healing Secondary to Iron Loading

We sought to address the changes in oxidative status and wound healing trajectories observed in iron-loaded skin through the induction of Nrf2 activity. Excisional wounds on iron-loaded mice treated with a topical Nrf2 activator exhibit near-normal healing, similar to the wounds on dextran-loaded mice (**see figure, Supplemental Digital Content 4**, which displays Nrf2-activating topical therapy, which reverts the wounding healing delay of iron-overloaded mouse skin. A, Schematic of Nrf2 activation by RTA 408 (inducer). **B,** Representative photographs of excisional wounds and treatments, n = 5 for all treatment groups. Keap-1 indicates Kelch-like ECH-associated protein-1, **http://links.lww.com/PRSGO/B440**) **(see figure, Supplemental Digital Content 5**, which displays Nrf2-activating therapy, which increases reepithelialization and expression of antioxidant and cytoprotective genes. A, Epithelial gap measured in pixels at day 10 postwounding. n = 3 for all treatment groups, **http://links.lww.com/PRSGO/B441**). Nrf2-activating topical therapy significantly reduces the pathologic time to closure in both IP and SC wound cohorts, a finding that holds for both 0.1% and 1.0% doses (Fig. 4A). For IP-loaded mouse wounds, both 0.1% and 1.0% RTA 408 reduced wound closure time by 108%, in comparison with vehicle-treated wounds (Fig. 4A). For the SC-loaded mouse wounds, 0.1% RTA 408reduced the pathological wound closure time by 128%, while 1.0% RTA 408 reduced the pathological

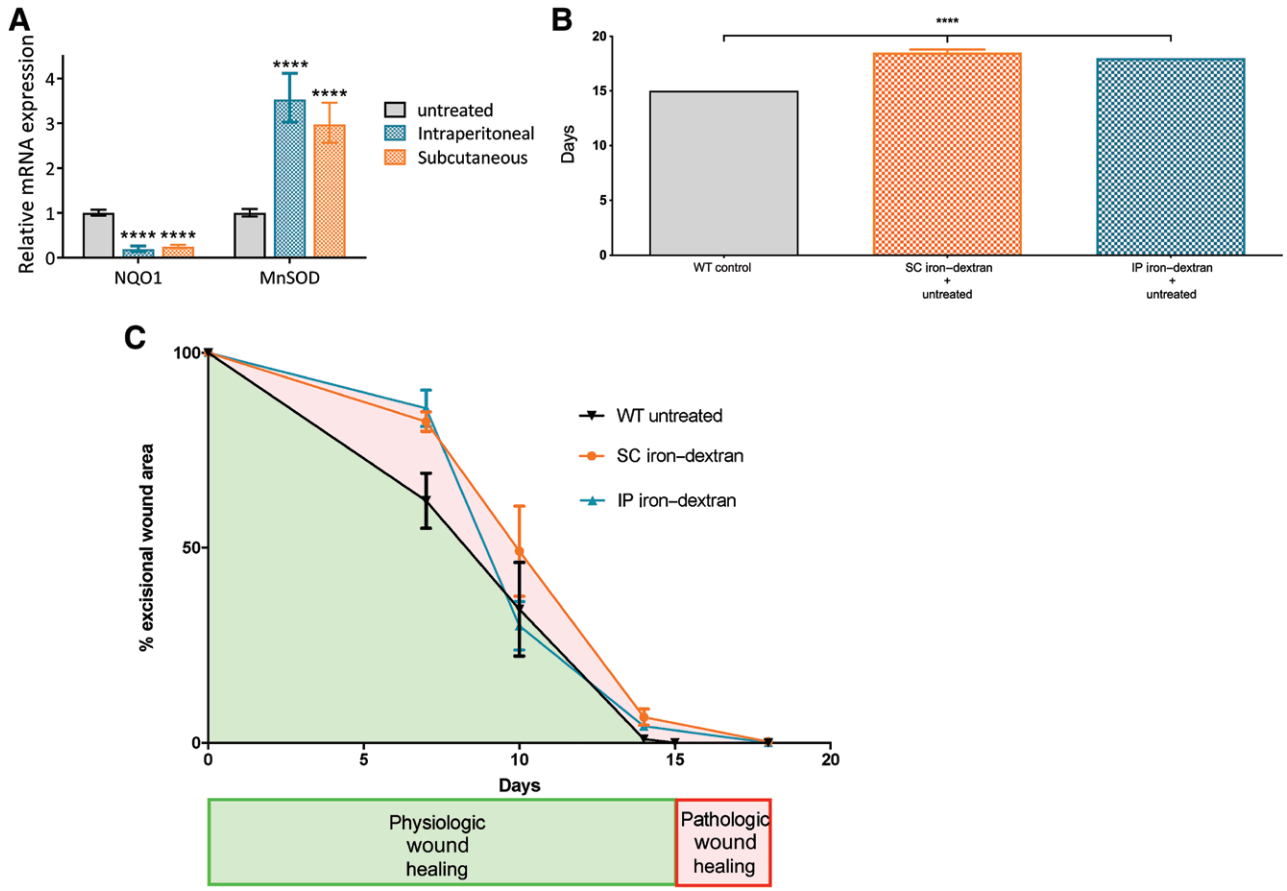

Fig. 3. Characterization of iron-loaded skin and establishment of a model for delayed wound healing secondary to chronic venous stasis. A, Relative mRNA expression levels of NQO1 and MnSOD for iron-loaded and dextran-loaded tissues. ****$P < 0.0001$. B, Average time to wound closure. ******$P < 0.0001$. C, Graph of percent excisional wound area over time, n = 5. D, Quantification of wound burden (area under curve) for each experimental arm.

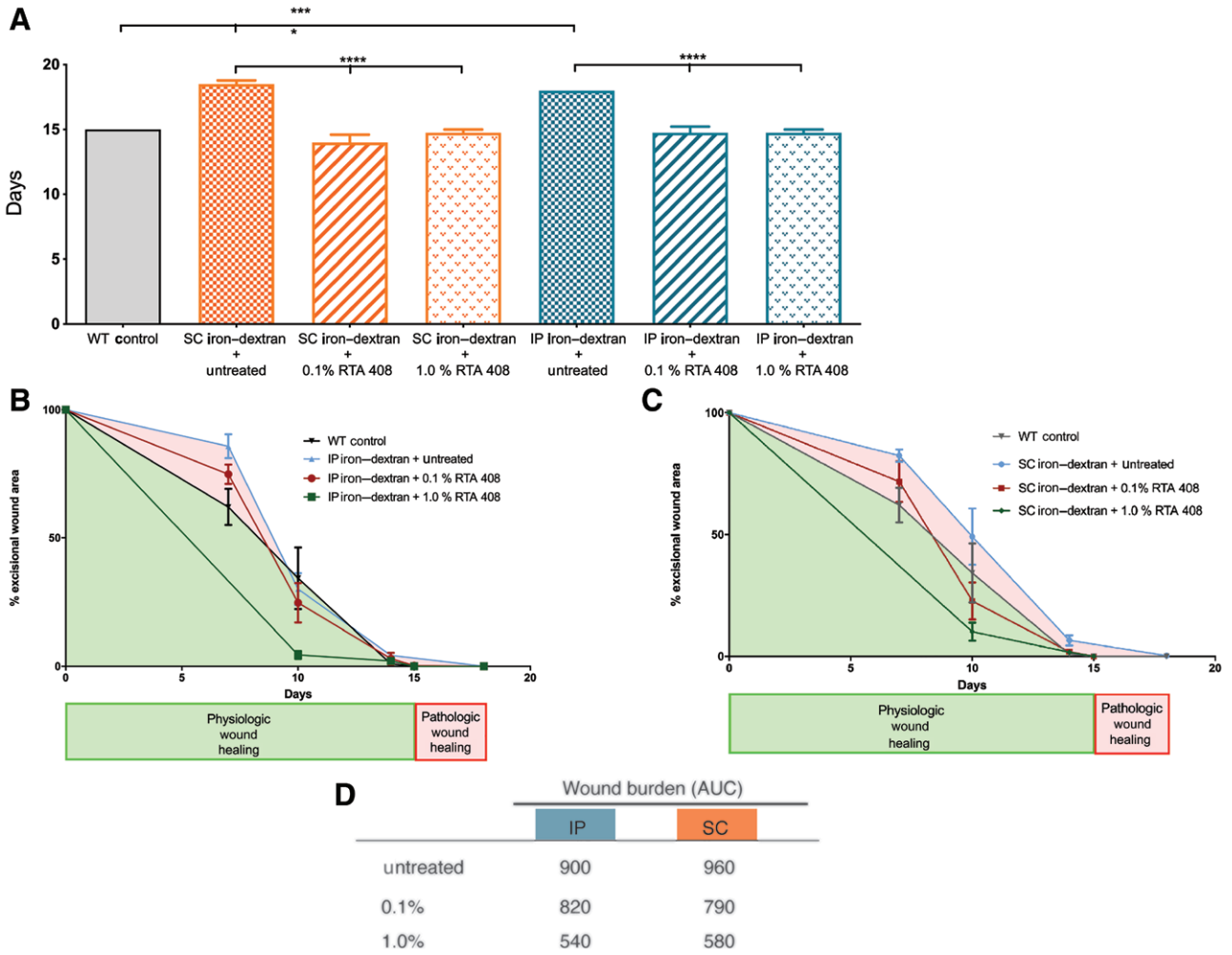

Fig. 4. Nrf2-activating topical therapy reverts the wounding healing delay of iron-overloaded mouse skin. A, Average time to wound closure. ***P* < 0.01; ****P* < 0.001; *****P* < 0.0001. B, Graph of percent excisional wound area over time for IP experimental arm. Pathologic wound burden (pink) = area under curve (IP—iron-dextran) − area under curve (dextran, physiologic wound burden in green). n = 5 for all treatment groups. C, Same as D but for SC experimental arm. D, Quantification of wound burden (area under curve).

time by 107%, compared with vehicle-treated wounds. Based on the plots of the remaining wound area over time, for the IP group, the 1.0% and 0.1% doses reduced the pathological wound burden by 307% and 69.3%, respectively, when compared with that of vehicle-treated IP-loaded wounds (Fig. 4B). For the SC group, the higher dose of Nrf2 activator again led to a dramatic reduction in pathological wound burden of 94% with 0.1% RTA 408 and 216% with 1.0% RTA 408, compared with vehicle-treated wounds (Fig. 4D,E). Our data suggest a remarkable benefit for Nrf2-activating topical therapy in iron-loaded skin modeling CVI pathology.

Antioxidant Gene Expression Is Significantly Restored by Topical Nrf2 Activation Therapy

Iron-loaded skin was previously noted to have a reduced expression of *NQO1* (Fig. 3A). For the IP cohort, *NQO1* is significantly increased with topical RTA 408 treatment (Fig. 5A). There appears to be a minor but insignificant dose response in expression levels when RTA 408 is increased from 0.1% to 1.0%. Levels of other antioxidant genes *MnSOD* and *HO-1* are similarly upregulated. Within the SC cohort, the expression levels of *NQO1*, *MnSOD*, and *HO-1* are higher with treatment, and there appears to be a dose response but without statistical significance (Fig. 5B). The increase in antioxidant expression levels may be more dramatic when iron loading is achieved systemically. RTA 408 treatment also led to increased epithelialization of day 10 wounds.

DISCUSSION

Venous ulcers are a cause of significant morbidity, and despite the large share of health expenses dedicated to their treatment, they often remain chronic and undertreated. The design of a reproducible animal model is attractive in this regard for ease in streamlining research and therapeutic design. Mice are readily accessible, cheap to purchase, and are easily cared for. While there are limitations in extrapolating findings to humans, the use of stents and other modifications helps circumvent some confounding factors.[27,29,30]

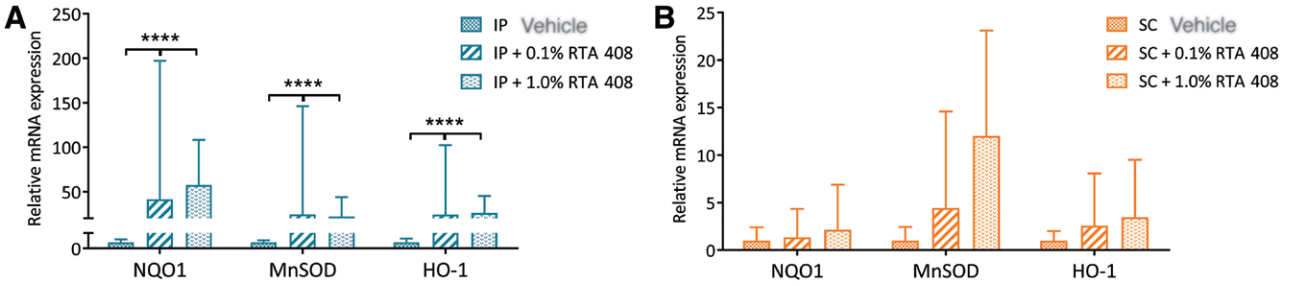

Fig. 5. Nrf2-activating therapy increases reepithelialization and expression of antioxidant and cytoprotective genes. A, Relative mRNA expression levels of *NQO1*, *MnSOD*, and *HO-1* in IP iron-loaded skin tissue following treatment of RTA 408. ****$P < 0.0001$. n = 6 for all treatment groups. B, Same as in A but for SC iron-loaded skin tissues.

We present findings from an adapted model for cutaneous would healing in the setting of iron overload. Importantly, the results corroborate the validity of the model in light of existing literature. Iron loading through intraperitoneal or subcutaneous means results in the accumulation of dense iron deposits in the skin layers in a manner that parallels human chronic venous stasis. However, subcutaneous iron loading is uniquely associated with increased dermal fibrosis, which is a well-documented finding in clinical reports of human CVI.[31,32] Systemic iron loading through intraperitoneal means is therefore more limited in its applicability as a model for human chronic venous stasis. Dense fibrosis of the skin is a feature of the local inflammatory response in CVI and a likely contributor to skin complications. Iron overloading leads to delayed healing, as expected, and the potential rescue of the pathologic process is accomplished through Nrf2-mediated antioxidant gene expression. The latter finding supports the current evidence that iron overload leads to increased ROS and pathophysiology across multiple organs.[33–38] Free iron has been shown to increase ROS accumulation through the Fenton reaction and macrophage processing of iron complexes, both of which contribute to lipid peroxidation and ferroptosis. Nrf2 may restore redox balance in the setting of iron overload by transcriptionally upregulating key enzymes that regenerate reducing equivalents, directly quench ROS, and prevent ferroptosis of cells in the wound bed.

There are a number of limitations to this study. The model is based on features specific to more advanced CVI, where iron overload is one of the several important chronic changes within cutaneous tissues. While the accumulation of iron is likely a local driver of M1 macrophage activity and the ensuing inflammation, tissue degradation, and fibrosis, there are likely to be other relevant features of chronic wounds in CVI that are independent of iron overload. Consequently, the model can be used to study inflammatory and oxidative changes resulting from cutaneous iron overload but may not well represent other contributors like local hypertension, tissue hypoxia, and endothelial dysfunction. The method for dispersing iron dextran within the subcutaneous tissue is variable when compared with systemic means of delivery, and this point is an important consideration when measuring skin findings in this model. To address this limitation, it is necessary to inject the dilute iron–dextran across a wide area of the skin to avoid aggregated deposits. Despite these shortcomings, the subcutaneous injection of iron more specifically models CVI's distribution of iron overload, which accumulates in the skin and soft tissues. Intraperitoneal injection of iron more closely resembles systemic iron-overload disorders, such as hemochromatosis, where iron accumulates throughout the body and may have untoward effects on other organ systems.

Future directions involve the continued use and adaptation of the proposed model based on advancing research in the field of CVI. Heritable traits can be easily manipulated with a mouse model, and they can be subsequently investigated with regard to iron-overload handling or redox imbalance. Topical and systemic therapies can be quickly tested and with a robust analysis of cellular markers. The excisional model is easily quantified and therefore translates well to scientific analysis in many forms.

CONCLUSIONS

We propose a novel model for the study of impaired cutaneous wound healing in CVI using subcutaneous iron loading. Buildup of iron skin deposits is associated with redox imbalance and delayed wound healing that are corrected by topical administration of a potent Nrf2 activator. Our study describes a reproducible model to study a common clinical entity and demonstrates its utility in the advancement of therapeutic means.

Daniel J. Ceradini, MD
Hansjörg Wyss Department of Plastic Surgery
NYU Langone Health
540 1st Avenue, Lab 2-3
New York, NY 10016
E-mail: daniel.ceradini@nyulangone.org

Piul S. Rabbani, PhD
Hansjörg Wyss Department of Plastic Surgery
NYU Langone Health
540 1st Avenue, Lab 2-3
New York, NY 10016
E-mail: piul.rabbani@nyulangone.org

ACKNOWLEDGMENTS

We acknowledge NYU Langone's Experimental Pathology Research Laboratory, which is partially supported by the Cancer Center Support Grant P30CA016087 at the Laura and Isaac Perlmutter Cancer Center.

REFERENCES

1. Rabe E, Pannier F. Societal costs of chronic venous disease in CEAP C4, C5, C6 disease. *Phlebology.* 2010;25(suppl 1):64–67.
2. Davies AH. The seriousness of chronic venous disease: a review of real-world evidence. *Adv Ther.* 2019;36(suppl 1):5–12.
3. Moore HM, Lane TR, Thapar A, et al. The European burden of primary varicose veins. *Phlebology.* 2013;28(suppl 1):141–147.
4. Rabe E, Guex JJ, Puskas A, et al; VCP Coordinators. Epidemiology of chronic venous disorders in geographically diverse populations: results from the Vein Consult Program. *Int Angiol.* 2012;31:105–115.
5. Zolotukhin IA, Seliverstov EI, Shevtsov YN, et al. Prevalence and risk factors for chronic venous disease in the general Russian population. *Eur J Vasc Endovasc Surg.* 2017;54:752–758.
6. Robertson L, Lee AJ, Evans CJ, et al. Incidence of chronic venous disease in the Edinburgh Vein Study. *J Vasc Surg Venous Lymphat Disord.* 2013;1:59–67.
7. Danielsson G, Eklof B, Grandinetti A, et al. The influence of obesity on chronic venous disease. *Vasc Endovascular Surg.* 2002;36:271–276.
8. Mahapatra S, Ramakrishna P, Gupta B, et al. Correlation of obesity & comorbid conditions with chronic venous insufficiency: results of a single-centre study. *Indian J Med Res.* 2018;147:471–476.
9. Weller CD, Gardiner EE, Arthur JF, et al. Autologous platelet-rich plasma for healing chronic venous leg ulcers: clinical efficacy and potential mechanisms. *Int Wound J.* 2019;16:788–792.
10. Mutlak O, Aslam M, Standfield NJ. Chronic venous insufficiency: a new concept to understand pathophysiology at the microvascular level—a pilot study. *Perfusion.* 2019;34:84–89.
11. Pocock ES, Alsaigh T, Mazor R, et al. Cellular and molecular basis of venous insufficiency. *Vasc Cell.* 2014;6:24.
12. Mansilha A, Sousa J. Pathophysiological mechanisms of chronic venous disease and implications for venoactive drug therapy. *Int J Mol Sci.* 2018;19(6):1669.
13. Castro-Ferreira R, Cardoso R, Leite-Moreira A, et al. The role of endothelial dysfunction and inflammation in chronic venous disease. *Ann Vasc Surg.* 2018;46:380–393.
14. Katsenis K. Micronized purified flavonoid fraction (MPFF): a review of its pharmacological effects, therapeutic efficacy and benefits in the management of chronic venous insufficiency. *Curr Vasc Pharmacol.* 2005;3:1–9.
15. Nikfarjam BA, Adineh M, Hajiali F, et al. Treatment with rutin—a therapeutic strategy for neutrophil-mediated inflammatory and autoimmune diseases: anti-inflammatory effects of rutin on neutrophils. *J Pharmacopuncture.* 2017;20:52–56.
16. MacLennan WJ, Wilson J, Rattenhuber V, et al. Hydroxyethylrutosides in elderly patients with chronic venous insufficiency: its efficacy and tolerability. *Gerontology.* 1994;40(1):45–52.
17. Wilkinson LS, Bunker C, Edwards JC, et al. Leukocytes: their role in the etiopathogenesis of skin damage in venous disease. *J Vasc Surg.* 1993;17:669–675.
18. Herouy Y, May AE, Pornschlegel G, et al. Lipodermatosclerosis is characterized by elevated expression and activation of matrix metalloproteinases: implications for venous ulcer formation. *J Invest Dermatol.* 1998;111:822–827.
19. Handa P, Thomas S, Morgan-stevenson V, et al. Iron alters macrophage polarization status and leads to steatohepatitis and fibrogenesis. *J Leukoc Biol.* 2019;105:1015–1026.
20. Ackerman Z, Seidenbaum M, Loewenthal E, et al. Overload of iron in the skin of patients with varicose ulcers. Possible contributing role of iron accumulation in progression of the disease. *Arch Dermatol.* 1988;124:1376–1378.
21. Caggiati A, Franceschini M, Heyn R, et al. Skin erythrodiapedesis during chronic venous disorders. *J Vasc Surg.* 2011;53(6):1649–1653.
22. Gemmati D, Federici F, Catozzi L, et al. DNA-array of gene variants in venous leg ulcers: detection of prognostic indicators. *J Vasc Surg.* 2009;50:1444–1451.
23. Zamboni P, Izzo M, Tognazzo S, et al. The overlapping of local iron overload and HFE mutation in venous leg ulcer pathogenesis. *Free Radic Biol Med.* 2006;40:1869–1873.
24. Wright JA, Richards T, Srai SK. The role of iron in the skin and cutaneous wound healing. *Front Pharmacol.* 2014;5:156.
25. Sochaski MA, Bartfay WJ, Thorpe SR, et al. Lipid peroxidation and protein modification in a mouse model of chronic iron overload. *Metabolism.* 2002;51:645–651.
26. Sindrilaru A, Peters T, Wieschalka S, et al. An unrestrained proinflammatory M1 macrophage population induced by iron impairs wound healing in humans and mice. *J Clin Invest.* 2011;121:985–997.
27. Galiano RD, Michaels J V, Dobryansky M, et al. Quantitative and reproducible murine model of excisional wound healing. *Wound Repair Regen.* 2004;12:485–492.
28. Rabbani PS, Ellison T, Waqas B, et al. Targeted Nrf2 activation therapy with RTA 408 enhances regenerative capacity of diabetic wounds. *Diabetes Res Clin Pract.* 2018;139:11–23.
29. Ansell DM, Holden KA, Hardman MJ. Animal models of wound repair: are they cutting it? *Exp Dermatol.* 2012;21(8):581–585.
30. Lindblad WJ. Considerations for selecting the correct animal model for dermal wound-healing studies. *J Biomater Sci Polym Ed.* 2008;19:1087–1096.
31. Choonhakarn C, Chaowattanapanit S, Julanon N. Lipodermatosclerosis: a clinicopathologic correlation. *Int J Dermatol.* 2016;55:303–308.
32. Caggiati A, Rosi C, Casini A, et al. Skin iron deposition characterises lipodermatosclerosis and leg ulcer. *Eur J Vasc Endovasc Surg.* 2010;40:777–782.
33. Sung HK, Song E, Jahng JWS, et al. Iron induces insulin resistance in cardiomyocytes via regulation of oxidative stress. *Sci Rep.* 2019;9(1):4668.
34. Tanaka H, Espinoza JL, Fujiwara R, et al. Excessive reactive iron impairs hematopoiesis by affecting both immature hematopoietic cells and stromal cells. *Cells.* 2019;8:226.
35. Ammar O, Houas Z, Mehdi M. The association between iron, calcium, and oxidative stress in seminal plasma and sperm quality. *Environ Sci Pollut Res Int.* 2019;26:14097–14105.
36. Mehta KJ, Farnaud SJ, Sharp PA. Iron and liver fibrosis: mechanistic and clinical aspects. *World J Gastroenterol.* 2019;25:521–538.
37. Vinchi F, Porto G, Simmelbauer A, et al. Atherosclerosis is aggravated by iron overload and ameliorated by dietary and pharmacological iron restriction. *Eur Heart J.* 2019;41:2681–2695.
38. Hyeun JA, Kim JY, Kim CH, et al. Iron is responsible for production of reactive oxygen species regulating vasopressin expression in the mouse paraventricular nucleus. *Neurochem Res.* 2019;44:1201–1213.